IEEE Access
Multidisciplinary | Rapid Review | Open Access Journal

SPECIAL SECTION ON GREEN INTERNET OF THINGS

Received December 24, 2019, accepted January 9, 2020, date of publication January 20, 2020, date of current version February 19, 2020.

Digital Object Identifier 10.1109/ACCESS.2020.2966510

Hybrid Seismic-Electrical Data Acquisition Station Based on Cloud Technology and Green IoT

SHUAIQING QIAO[1], QISHENG ZHANG[1], QIMAO ZHANG[2], FENG GUO[1], AND WENHAO LI[1]

[1]School of Geophysics and Information Technology, China University of Geosciences at Beijing, Beijing 100192, China
[2]Institute of Electronics, Chinese Academy of Sciences, Beijing 100010, China

Corresponding author: Qisheng Zhang (zqs@cugb.edu.cn)

This work was supported in part by the Natural Science Foundation of China under Grant 41574131, in part by the National Key Research and Development Program of China under Grant 2017YFF0105704, in part by the National "863" Program of China under Grant 2012AA06110203, in part by the PetroChina Innovation Foundation under Grant 2019D-5007-0302, and in part by the Fundamental Research Funds for the Central Universities of China.

ABSTRACT Traditional geophysical prospecting instruments cannot fulfill the requirements of deep energy prospecting. The instruments that measure single physical quantities, such as seismic and electrical instruments, have certain limitations. Moreover, the time period required for traditional instruments to collect, acquire, and process data is too long. To address these issues, a hybrid seismic-electrical data acquisition system based on cloud technology and green IoT was proposed and developed. A seismic analog acquisition circuit and an electrical analog acquisition circuit were designed, and the control module was designed and debugged. The system is equipped with a wireless module connected to a wireless-to-4G/5G module, which uploads the data collected by the hybrid seismic-electrical data acquisition station to the cloud platform. The background master control center completes the rapid processing of geophysical data using the robust storage and computing capabilities of the cloud. Meanwhile, it sends control commands to the cloud to control the acquisition system. This system has completed simultaneous prospecting of multiple physical quantities and achieved rapid monitoring through cloud technology. Finally, the system was used to perform fracture monitoring and a comparison of two mines in Daqing City, Heilongjiang Province. The monitoring results were satisfactory. Thus, the presented system can play a role in seismic-electrical prospecting, and can be applied to actual engineering endeavors quickly and reliably.

INDEX TERMS 4G/5G, cloud platform, geophysics, hybrid seismic-electrical,green IoT.

I. INTRODUCTION

Ninety percent of the energy used worldwide is derived from fossil fuels, i.e., coal, oil, and natural gas, and more than 80% of industrial raw materials are derived from metal and non-metallic mineral resources [1], [2]. Presently, the proven recoverable oil reserves on earth can be used for only 45 to 50 years [3], and the total natural gas reserves, which are 18 billion cubic meters, may be available for the next 50 to 60 years [4], [5]. Moreover, the coal reserves can be used for the next 200 to 300 years [6], [7], and the primary metal and non-metallic minerals may be available for decades or more than 100 years. Furthermore, energy consumption has dramatically increased in recent years [8]–[11]. Therefore, detection of unproven fossil energy sources and the development and utilization of new energy resources are critical [12]. Currently, prospecting and mining of mineral resources mainly rely on geophysical prospecting [13]. Factors required for its development include the advancement of precision instruments [14], data recovery methods, and data processing and interpretation methods.

In terms of data processing and interpretation, geophysicists have had to grapple with the myriad solutions that exist for a single geophysical prospecting method, a problem that also exists in geophysical prospecting [15]. To solve this problem, multi-method joint prospecting has become an active research topic [16]. Among geophysical prospecting methods, seismic and electrical prospecting techniques have been widely applied; however, they have both advantages and limitations. The physical property parameters of seismic prospecting research are mainly seismic wave velocities [17], while the physical property parameter of electrical research is primarily resistivity [18], [19]. Experiments have shown that vibration of the underground medium will cause a slight

The associate editor coordinating the review of this manuscript and approving it for publication was Jun Wu.

change in its electrical structure, which is known as the seismoelectric effect. To better address the strengths and weaknesses of seismic and electrical prospecting methods by forming complementary approaches, reducing the multiplicity of solutions, and improving the reliability of prospecting results, new breakthroughs have been made in the study of the seismoelectric effect. The need for multi-method joint prospecting research has thus become critical [20], [21].

With respect to instrument design, as well as data recovery and processing, use of prospecting instruments and the recovery and processing of data are difficult because of the complex terrain encountered by current energy prospecting. Furthermore, prospecting and has become increasingly more difficult. However, owing to the rapid development of internet technologies in recent years [22], [23], the cloud platform [24], big data [25], [26], and other technologies have gradually matured. Prompted by the science and technology of developed countries and the promotion by market trends, the combination of the Internet of Things (IoT) and cloud platform applications have shown unprecedented development. IoT with the cloud platform has begun to rapidly integrate with conventional industrial technologies [27]–[29]. Endeavors such as big data calculation [30], green IoT,comprehensive interpretation, safety inspection [31], [32], geological modeling [33], dynamic analysis, oil production engineering, and drilling tests involve a significant amount of data and concomitant data processing problems. Incorporating cloud technology into the existing wireless network building platform can be greatly beneficial.

By combining the two issues mentioned above, the present research team developed a high-precision hybrid seismic-electrical data acquisition system based on cloud technology. This system simultaneously collects seismic and electrical signals. The acquisition station is small in size, light in weight, and convenient to carry. It is equipped with a wireless transmission system [34]. After conversion from wireless to 4G/5G, the signals are sent to the cloud platform. With the powerful storage capabilities and excellent computing capabilities of the cloud platform [35], a large amount of geophysical data can be stored and computed in a short time, providing an effective platform for online monitoring [36]. This concept and technology can serve as a basis for the prediction of natural disasters such as earthquakes [37].

II. ACQUISITION STATION STRUCTURE DESIGN

A. OVERALL ACQUISITION STATION HARDWARE STRUCTURE

The hybrid seismic-electrical data acquisition system is the basic acquisition unit of the proposed design. Fig. 1 shows the basic structural framework of the acquisition station. The vibration signals are converted into analog electrical signals through first-stage geophones and they are transmitted to the acquisition end. The electrical signals are transmitted to the acquisition end through electrodes. In the second stage, the signals are pre-processed by filtering and other tasks.

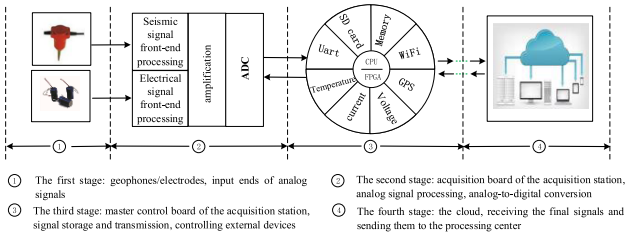

FIGURE 1. Overall structural framework of the acquisition station.

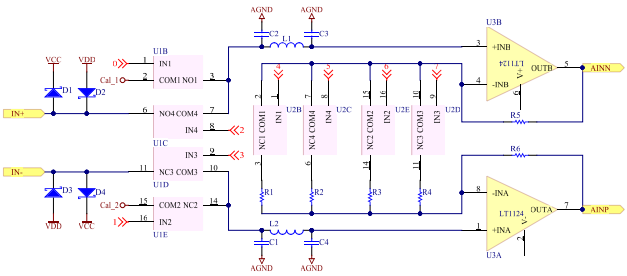

FIGURE 2. Front-end processing circuit of the acquisition-station electrical data acquisition path.

Hence, their respective front-end processing circuits, and the post-processing signals are amplified. Then, the analog signals are converted into digital signals by an analog-to-digital conversion chip. The converted digital signals enter the third-stage master control part of the acquisition system, where the final digital filtering and storage processes are completed. The signals are then transmitted to the next stage, the cloud server.

B. DESIGN OF THE FRONT-END ACQUISITION CIRCUIT

In the acquisition station, the effective frequency bands of the collected seismic signals are predominantly at low frequencies, with a range of 0–200 Hz. It is therefore essential to perform low-pass filtering on signals of the geophones at the analog end of the acquisition station. The electrical methods include various types. The electrical signals of different frequency bands can be collected for different analysis and inversion methods. In this design, the electrical method of data acquisition also collects the low-frequency electrical signals because they decay more slowly and propagate for a longer distance in the ground. These signals, combined with seismic signals, are beneficial for making judgments on changes in the underground medium.

Fig. 2 depicts the front-end processing circuit of the acquisition station electrical-data acquisition path. In this figure, IN+ and IN− are the signal input ends. A pair of clamping diodes is added at each end of the differential signal to control the amplitude of the input signal within the collector supply voltage and voltage drain supply (VCC-VDD). This helps prevent damage of the internal circuit caused by external large signals. Chips U_1 and U_2 are two analog switch chips. Each chip contains four analog switches. U_{1B} and U_{1E} control

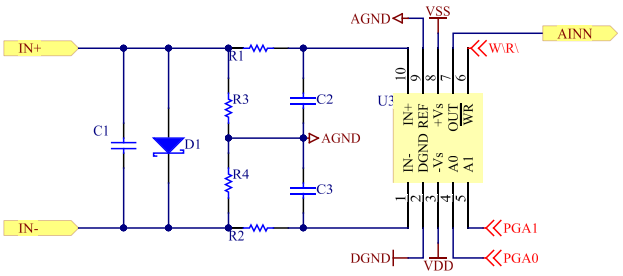

FIGURE 3. Front-end processing circuit of the acquisition-station seismic data acquisition path.

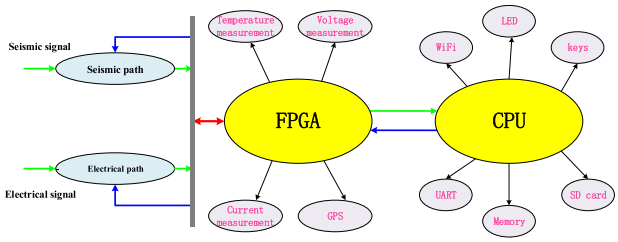

FIGURE 4. Structure of the master control circuit.

the input of the self-test signal of the acquisition station, and U_{1C} and U_{1D} control the input of the signal returned by the electrodes. After the signal enters the circuit, it first goes through two symmetrical LC-π type filters to filter out the common-mode and high-frequency components in the signal. The filtered signal then enters a controllable instrumentation amplifier consisting of two amplifiers and multiple resistors. Amplification factor A is as follows (into the circuit):

$$A = 1 + \frac{2 \times R5}{R} \tag{1}$$

where R5 = R6, and R is the parallel resistance when R1, R2, R3 and R4 are connected. The amplified signal is further processed by the subsequent circuit. It then enters the AD circuit for analog-to-digital conversion, whereby the analog signal is converted into a digital signal.

Fig. 3 illustrates the front-end signal processing circuit of the seismic-data-acquisition path of the hybrid seismic-electrical data acquisition station. The front-end inputs IN+ and IN− of the circuit are connected to the cathode and anode of the geophone, respectively. The two ends of the output are connected to the positive and negative input ends of the post-stage instrumentation amplifier. D1 is a glass passivation junction transient-voltage suppressor, which protects the circuit and limits the input signal within a certain range. R3 and R4 are matching resistors at the input ends and are employed to implement impedance matching with the geophone. The bandwidth of the analog-to-digital converter is limited. Thus, to prevent aliasing, it is necessary to perform anti-alias filtering before sampling to filter out signals higher than the Nyquist frequency. Resistors R1 and R2 and capacitors C2 and C3 form a common-mode filter, which filters out high-frequency common-mode components in the input signal. Resistors R1 and R2 and capacitor C1 form a differential-mode filter, which is used to implement the low-pass filtering function. At the same time, C1 can reduce the impact of the mismatching between C2 and C3, thereby improving the circuit performance. After filtering, the signal is amplified by the U3 program-controlled amplifier. PGA0 and PGA1 input different control signals to manage different magnification factors of the amplifier. The chip can output four amplification factors.

C. MASTER CONTROL CIRCUIT DESIGN

The master control circuit of the acquisition station is used to control data collection, data storage, and human–machine interactions. In this system, the core processor is composed of ARM and FPGA. Through their coordination, a series of functions, such as acquisition-system detection, communication management, data storage, system control and configuration, clock synchronization, and human–machine interactions, are completed and implemented. In its functional realization, FPGA is mainly responsible for five tasks. The first task is to control the scheduling and execution of time-related tasks, including the generation of a sampling clock, the scheduling of related strategies, the generation of a real-time clock, and others. The second task is to control data collection from the voltage, current, temperature, and other sensors. The third task is to control the acquisition system and data buffering. The fourth one is to complete the wired data communication. Finally, FPGA is used for GPS information decoding and time synchronization. The detailed structure of the master control circuit is shown in Fig. 4.

After completing construction of the hardware in the master control circuit, a software program is required to drive it. The software runs on a Linux system platform that adopts a structured software design that is top-down, stepwise-refined. The overall software is designed according to a main thread. The main thread includes the respective data acquisition, instrument calibration, and data removal processes. It handles system status monitoring, LED display management, keypress management, network communications, and GPS decoding. The overall operation framework of the driving software of the master control module in the acquisition system is shown in Fig. 5.

III. NETWORKING STRUCTURE OF THE ACQUISITION STATION BASED ON THE CLOUD PLATFORM

The use and networking of acquisition stations are important for implementing field seismic-acquisition instruments. With the current complex environment and increasing difficulty of resource prospecting, various advanced requirements, such as those concerning earthquake resistance, crash resistance, high temperature resistance, and intelligence have been established for seismic instruments.

Following development of the distributed wireless microseismic data acquisition station, an innovative and convenient acquisition-station networking method is proposed based on

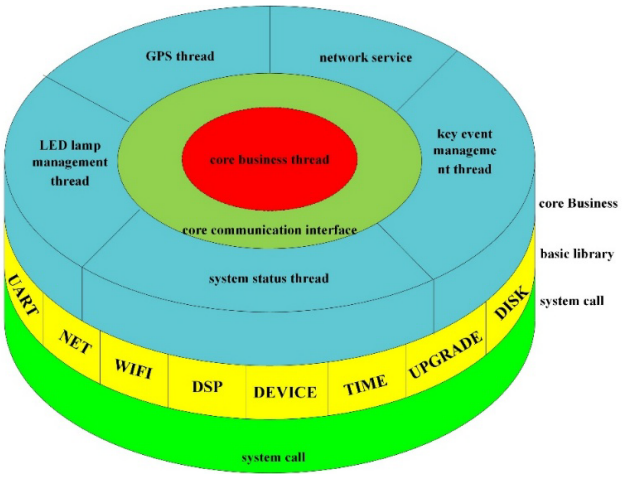

FIGURE 5. Overall structural framework of the software.

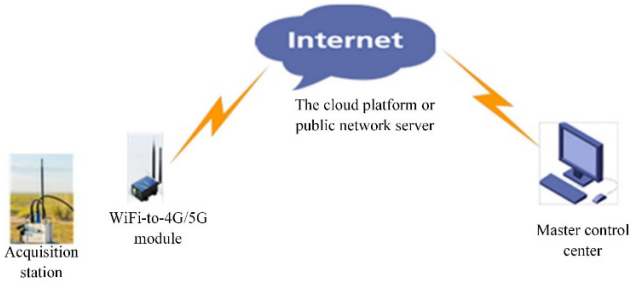

FIGURE 6. Schematic diagram of the acquisition-system field network.

the cloud platform. Fig. 6 presents a schematic diagram of the field network of the acquisition system. The front-end is an acquisition substation that processes the analog signals collected by geophones and converts them into digital signals for storage. It is connected to a WiFi conversion module that converts the WiFi signals into 4G/5G signals. The collected data can then be uploaded along the 4G/5G network to the central server and the cloud platform. Accordingly, the back-end equipment can arbitrarily download seismic and electrical data from the server for processing. Similarly, the back-end PC equipment can send control signals to the acquisition stations through the cloud platform.

In short, the proposed design combines cloud technology with the acquisition station network, thereby improving the acquisition-station network flexibility while making the field deployment easier in complex terrains. The collected data are thus conveniently received and processed.

IV. TEST COMPARING TWO MINES

A. THEORETICAL DERIVATION

The testing used in this study employs multiple self-developed acquisition stations. The monitoring analysis is mainly based on the data obtained from the seismic path; data from the electrical path are only used for post-assistant analysis. During the construction process, multiple acquisition stations are distributed at their corresponding positions around the fracturing well. The microseismic signals generated by the change of underground particle positions caused by fracturing are continuously recorded. This technology is used to map the hydraulic fractures in oil and gas reservoirs. The microseismic data during the fracturing process are continuously collected and processed to log the microseismic events, i.e., the locations of fractures. Owing to microseismic fracture diagnosis, it is possible to describe the direction and morphology of artificial fractures, effectively optimize fracturing and the fracturing scheme design, provide evaluations of reservoir resources, produce reservoir displacement information and recommended drilling location maps to achieve a better yield, and provide a basis for secondary prospect planning.

Microseismic events occur frequently underground. During hydraulic fracturing, the formation pressure increases. According to the Mohr–Coulomb criteria, microseisms will be induced in pressure-changing zones. The fracture profiles can be reflected by the distribution of the recorded microseismic focal locations. The theoretical basis of this technique is the Mohr–Coulomb criteria, whose mathematical expressions can be written as:

$$\tau \geq \tau 0 + \frac{S1 + S2 - 2P0}{2} + \frac{(S1 - S2)\cos 2\varphi}{2} \quad (2)$$

$$\tau = \frac{(S1 - S2)\sin 2\varphi}{2} \quad (3)$$

When the left side of (2) is not smaller than the right side, a microseism occurs. In this formula, τ is the shear stress acting on the fracture surface; $\tau 0$ is the inherent shear strength without normal stress of the rock whose value ranges from several MPa to tens of MPa, and its value is zero if the rock faults along an existing fracture surface. Additionally, S1 andS2 are the maximum and minimum principal stresses, respectively; P0 is the formation pressure; and φ denotes the angle between the maximum principle stress and the normal of the fracture surface. It is observed from (2) and (3) that microseisms tend to occur along existing fracture surfaces. Here, $\tau 0$ is zero, and the left side is usually not smaller than the right. By increasing P0, the right-side decreases, which makes the right side smaller than the left. This provides a basis for observations of hydraulic fractures. The testing uses eight acquisition stations with wireless transmission, a master station for recording, and real-time analysis and display. Monitoring is based on the microseismic focus characteristics, the seismic wave propagation theory, and the microseismic signal identification theory. The spatial distribution of the microseismic points and their three views are used to describe the profiles of artificial fractures, and the results of artificial fracture monitoring are provided.

The latest forward grid searching and positioning technology is applied to the microseismic focus location and signal identification. This technology can improve the reliability of microseismic focus location, and the signal identification can exclude human interference. A schematic diagram is shown in Fig. 7. To meet the positioning precision requirements, as well as to reduce the calculation amount and quickly

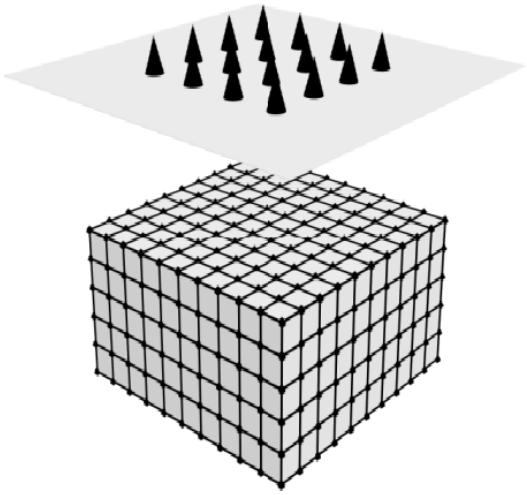

FIGURE 7. Schematic diagram of the station grid search and positioning.

produce results, a double-grid search technology is usually applied. In the first grid search, the grid spacing is large, such as 100 m, so that the number of nodes in the entire grid space is less than 10,000. The focus location obtained by the search is a node in the grid space with an error of 50 m. The second grid search is centered on the focus obtained in the first grid search. The error radius of the first grid search is used as the radius of the second grid space to build a search grid with 12.5 m grid spacing and 729 nodes. The second forward grid search and positioning is implemented with a theoretical error of 6 m, and the actual error is controlled at 10 m. Fig. 7 is a schematic diagram of the station grid search.

The time migration and related superposition theory of conventional seismic prospecting are introduced in the forward grid search and positioning technology. Further, more complicated velocity models can be applied, which improves the monitoring reliability.

B. DATA ANALYSIS AND COMPARISON OF TWO MINES

After completing the preparation work, the hydraulic fracturing process of the Lianhe-01 Mine and Lianhe-02 Mine are monitored using the acquisition stations. The physical parameters of the two mines are presented in Table 1. The hydraulic fracturing operation will cause a change in the underground stress field, resulting in microseismic waves generated by the fracturing or fault of the rock formation. This fracturing occurs in one layer, and the fracture monitoring record lasts 120 min. The location and magnitude of the microseismic events are retrieved through inversion by their identification and location.

The proposed approach uses a flat microseismic station network, a distributed network of acquisition stations, and a cloud transmission method. The coordinates in Figs. 8 and 9 use the projection of the hydraulic fracturing operation layer on the ground as the origin of the coordinates. The horizontal axis is in the east–west (EW) direction, and the E direction is positive. The vertical axis is in the north–south (NS)

TABLE 1. Physical parameters of the tested mines.

	Lianhe-01 Mine	Lianhe-02 Mine
Layer range/m	3114.9-3130.3	3120.0
Vertical depth/m	2680.4-2727.0	2598.71

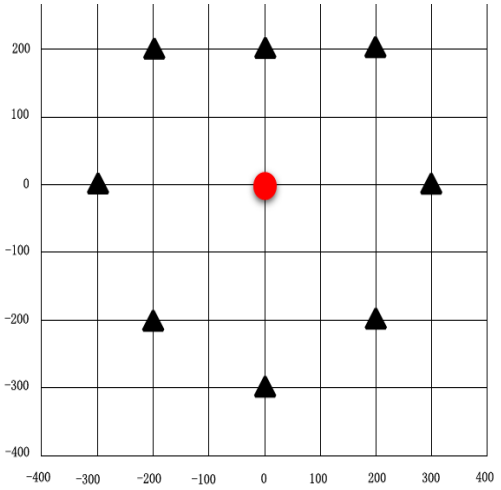

FIGURE 8. Monitoring station distribution map of Lianhe-01 Mine.

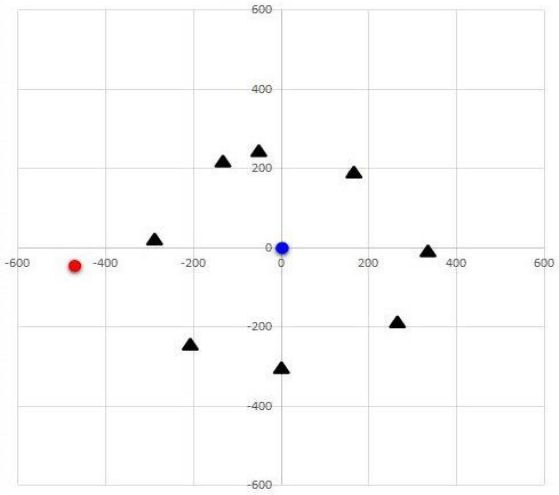

FIGURE 9. Monitoring station distribution map of Lianhe-02 Mine.

direction and the N direction is positive. The red dots in the figures indicate the positions of wellheads, and the black triangles represent the positions of geophones. More than eight acquisition stations in the test are placed on the ground and cut the monitoring area into a three-dimensional grid (Fig. 7). Before monitoring, the travel time of seismic waves from each node of the spatial grid to all monitoring stations are calculated.

The travel time differences from a certain node to a designated monitoring station and to other monitoring stations are given. During monitoring, a time difference correction is

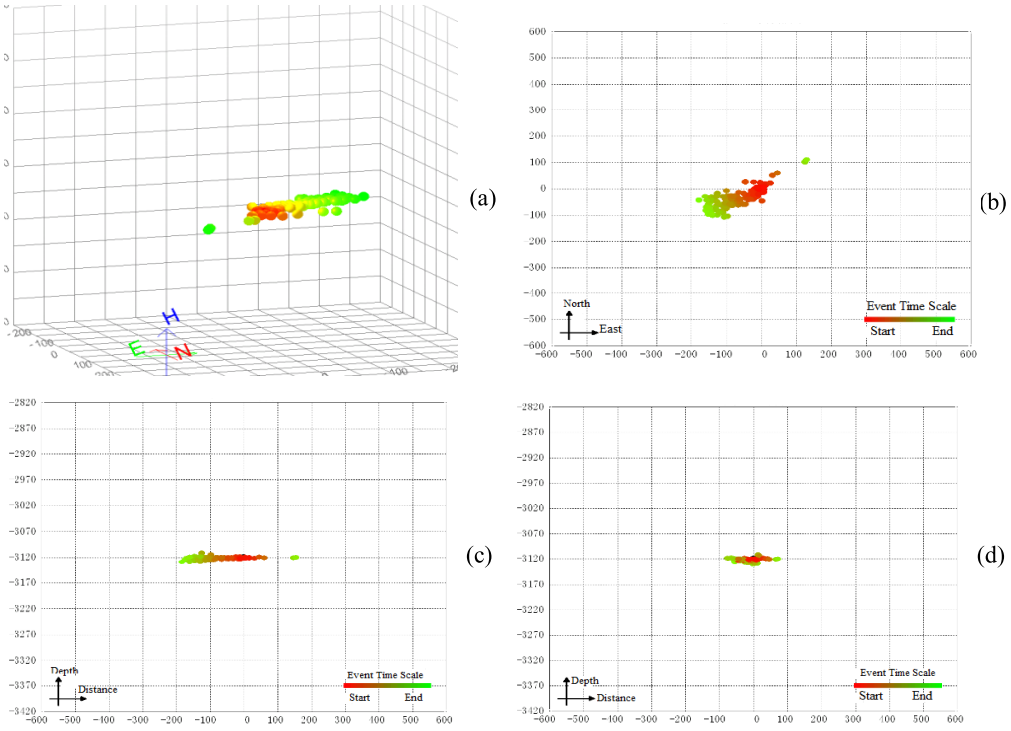

FIGURE 10. Inversion results of fracturing monitoring for Lianhe-01 Mine in (a) four-dimensional perspective view, (b) top view, (c) side view perpendicular to the fracturing direction, and (d) side view along the fracturing direction.

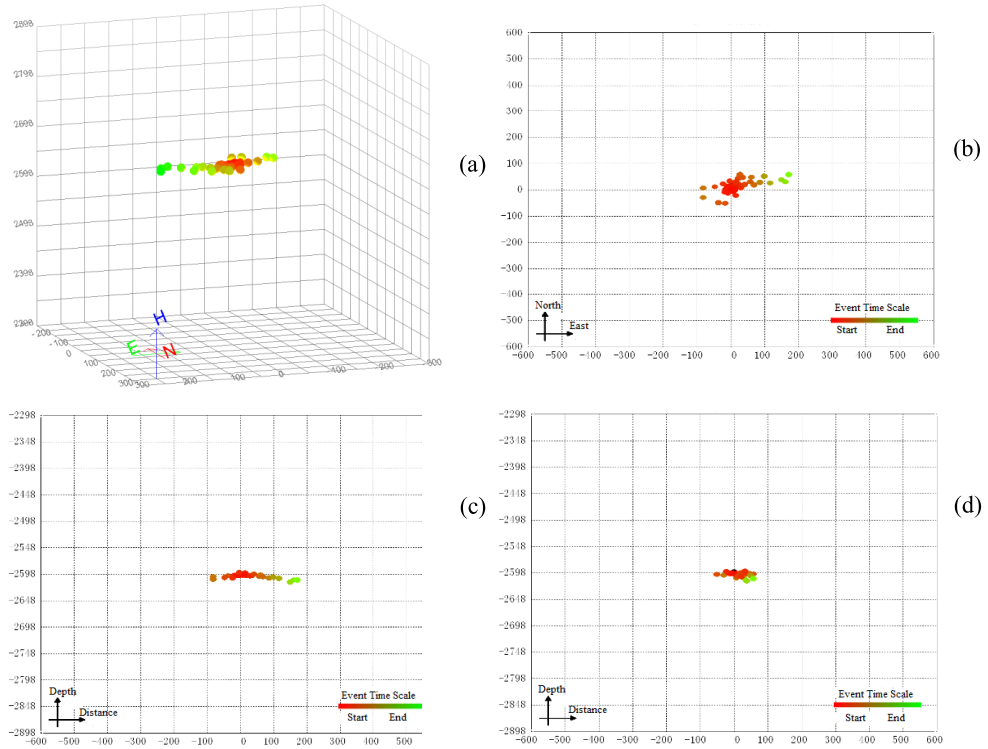

FIGURE 11. Inversion results of fracture monitoring for Lianhe-02 Mine in a (a) four-dimensional perspectival view, (b) top view, (c) side view perpendicular to the fracturing direction, and (d) side view along the fracturing direction.

performed on the seismic records of other stations. The results are superimposed on the seismic record of the designated station. If the amplitude of the superimposed seismic record significantly increases in a certain time period, and the signal becomes clearer, then there exists a seismic signal from this node. The use of time migration and microseismic record

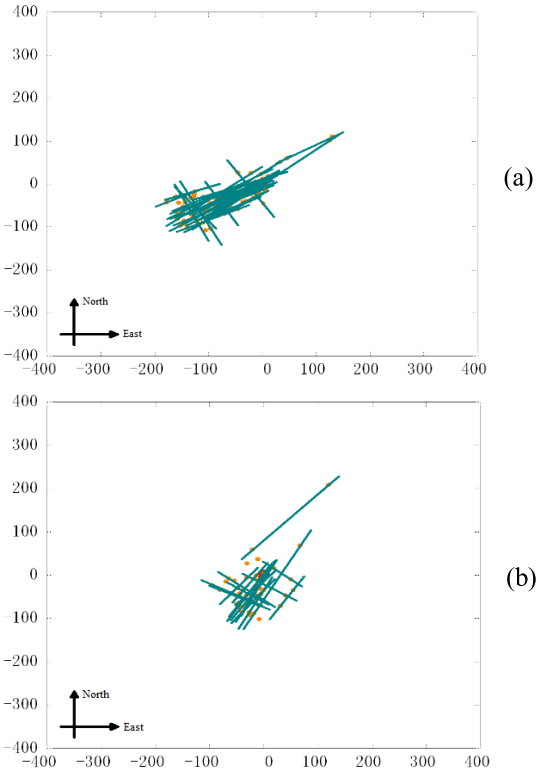

FIGURE 12. Structural analysis of the strike of the original fracture in (a) Lianhe-01 Mine and (b) Lianhe-02 Mine.

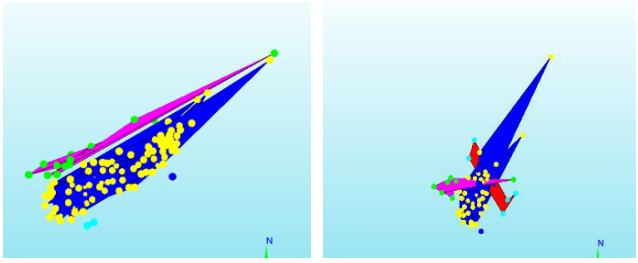

FIGURE 13. Three-dimensional top views of the hydraulic fractures of (a) Lianhe-01 Mine and (b) Lianhe-02 Mine.

superposition techniques can greatly improve the precision of spatial positioning and control the focus positioning error within 10 m. Figs. 10 and 11 illustrate four-dimensional perspectival views and three side views of fracture monitoring retrieved through inversion of the monitoring data of Lianhe-01 Mine and Lianhe-02 Mine, respectively.

According to analysis of data from the test results, the strike of the artificial fractures in Lianhe-01 Mine hydraulic fracturing is 62.7° northeast (NE), and the total fracture length is 339.7 m. The length of the west-wing water inflow fracture of the hydraulic fracturing is 171.3 m, and the length of the east-wing water inflow fracture is 168.4 m. The fracture height is 15.75 m, and the effective height of the water inflow fracture is 12.0 m. The near-mine original fractures are moderately developed, striking from 60–70° NE and 20–30° northwest (NW) and dipping 8° toward the NW on average. The strike of the artificial fractures in Lianhe-02 Mine hydraulic fracturing is 73.4° NE, and the total fracture length is 264.5 m. The length of the west-wing water inflow fracture of the hydraulic fracturing is 73.4 m; the length of the east-wing water inflow fracture is 191.1 m; and the height of the water inflow fracture is 12.3 m. The near-mine original fractures are moderately developed, striking from 60–80° NE and 10–30° NW and dipping 2° toward the SE on average. Figs. 12 and 13 are structural analysis diagrams and three-dimensional top views of the strikes of the original fractures respectively obtained by final processing of the monitoring data of the two mines.

V. CONCLUSION

In this paper, a design method of a hybrid seismic-electrical data acquisition system based on the cloud platform was proposed. A corresponding acquisition station that was developed based on the proposed methodology was introduced. The design and implementation of the front-end seismic data acquisition circuit were presented, along with the electrical data acquisition circuit and the master control circuit of the acquisition system. The structure of the acquisition-station driving software was described. Next, the acquisition-station networking method and the approach to implementing the cloud platform were detailed. In addition,

REFERENCES

[1] D. J. Wales, "Exploring energy landscapes," *Annu. Rev. Phys. Chem.*, vol. 69, no. 1, pp. 401–425, Apr. 2018.
[2] Y. Geng, J. Sarkis, and R. Bleischwitz, "How to globalize the circular economy," *Nature*, vol. 565, no. 7738, pp. 153–155, Jan. 2019.
[3] W. Ahmad, A. Adeel, and P. A. Tisman, "Oil consumption and economic growth: Evidence from Pakistan," *Energy Sour. B, Econ., Planning Policy*, vol. 13, no. 2, pp. 103–108, 2018.
[4] M. Skuzovatov, "Natural gas and condensate reserves in the Angara-Lena gas-bearing region," *Russian Geol. Geophys.*, vol. 58, nos. 3–4, pp. 503–515, Apr. 2017.
[5] Z. Hao, H. Fei, Q. Hao, and S. Turner, "Significant increase of oil and natural gas reserves throughout 2013," *Acta Geologica*, vol. 88, no. 2, p. 718, Apr. 2014.
[6] Z. Liu, D. B. Guan, H. Lee, and S. Moore, "Steps to China's carbon peak," *Nature*, vol. 522, no. 7556, pp. 279–281, 2015.
[7] S. Dai and R. B. Finkelman, "Coal geology in China: An overview," *Int. Geol. Rev.*, vol. 60, nos. 5–6, pp. 531–534, Apr. 2018.
[8] M. Schmidt, "Scarcity and environmental impact of mineral resources—An old and never-ending discussion," *Resources*, vol. 8, no. 1, p. 2, Dec. 2018.
[9] J. K. Jacka, "The anthropology of mining: The social and environmental impacts of resource extraction in the mineral age," *Annu. Rev. Anthropol.*, vol. 47, no. 1, pp. 61–77, Oct. 2018.
[10] S. A. Northey, G. M. Mudd, and T. T. Werner, "Unresolved complexity in assessments of mineral resource depletion and availability," *Nature Resour. Res.*, vol. 27, no. 2, pp. 241–255, Apr. 2018.
[11] E. De Cian and I. S. Wing, "Global energy consumption in a warming climate," *Environ. Resour. Econ.*, vol. 72, no. 2, pp. 365–410, 2019.
[12] M. Kivinen, J. Pokki, and M. Markovaara-Koivisto, "Discovered and undiscovered mineral resources: Evolving accounts and future prospects of minerals in Finland," *Mineral Econ.*, vol. 31, no. 3, pp. 301–317, Oct. 2018.
[13] M. Dentith, H. Yuan, S. Johnson, R. Murdie, and P. Piña-Varas, "Application of deep-penetrating geophysical methods to mineral exploration: Examples from Western Australia," *Geophysics*, vol. 83, no. 3, pp. WC29–WC41, May 2018.

[14] E. Serpelloni, C. Faccenna, G. Spada, D. Dong, and S. D. P. Williams, "Vertical GPS ground motion rates in the Euro-Mediterranean region: New evidence of velocity gradients at different spatial scales along the Nubia-Eurasia plate boundary," *J. Geophys. Res. Solid Earth*, vol. 118, no. 11, pp. 6003–6024, Nov. 2013.

[15] Z. Qi-sheng, D. Ming, W. Qi, F. Yong-Qiang, L. Wei-bing, and G. Jian, "Development of a new seismic-data acquisition station based on system-on-a-programmable-chip technology," *Ann. Geophys.*, vol. 56, no. 3, 2013, Art. no. 0329.

[16] S. Qiao, H. Duan, Q. Zhang, Q. Zhang, S. Li, S. Liu, S. Liu, Y. Wang, S. Yan, W. Li, and F. Guo, "Development of high-precision distributed wireless microseismic acquisition stations," *Geosci. Instrum. Methods Data Syst.*, vol. 7, no. 3, pp. 253–263, Sep. 2018.

[17] J. C. Hawthorne, M. Simons, and J. Ampuero, "Estimates of aseismic slip associated with small earthquakes near San Juan Bautista, CA," *J. Geophys. Res. Solid Earth*, vol. 121, no. 11, pp. 8254–8275, Nov. 2016.

[18] E. Sarafian, R. L. Evans, M. G. Abdelsalam, E. Atekwana, J. Elsenbeck, A. G. Jones, and E. Chikambwe, "Imaging precambrian lithospheric structure in Zambia using electromagnetic methods," *Gondwana Res.*, vol. 54, pp. 38–49, Feb. 2018.

[19] A. A. S. Barfod, I. Møller, A. V. Christiansen, A.-S. Høyer, J. Hoffimann, J. Straubhaar, and J. Caers, "Hydrostratigraphic modeling using multiple-point statistics and airborne transient electromagnetic methods," *Hydrol. Earth Syst. Sci.*, vol. 22, no. 6, pp. 3351–3373, Jun. 2018.

[20] I. Demirci, Ü. Dikmen, and M. E. Candansayar, "Two-dimensional joint inversion of magnetotelluric and local earthquake data: Discussion on the contribution to the solution of deep subsurface structures," *Phys. Earth Planet. Interiors*, vol. 275, pp. 56–68, Feb. 2018.

[21] M. Geng, Q. Yang, and D. Huang, "3D joint inversion of gravity-gradient and borehole gravity data," *Explor. Geophys.*, vol. 48, no. 2, pp. 151–165, 2017.

[22] X. Jing, Z. Yan, and W. Pedrycz, "Security data collection and data analytics in the Internet: A survey," *IEEE Commun. Surveys Tuts.*, vol. 21, no. 1, pp. 586–618, 1st Quart., 2019.

[23] G. Li, G. Xu, A. K. Sangaiah, J. Wu, and J. Li, "EdgeLaaS: Edge learning as a service for knowledge-centric connected healthcare," *IEEE Netw.*, vol. 33, no. 6, pp. 37–43, Nov. 2019.

[24] J. Ran, K. Hou, K. Li, and N. Dai, "A high security distance education platform infrastructure based on private cloud," *Int. J. Emerg. Technol. Learn.*, vol. 13, no. 10, p. 42, Oct. 2018.

[25] S. Pouyanfar, Y. Yang, S.-C. Chen, M.-L. Shyu, and S. S. Iyengar, "Multimedia big data analytics: A survey," *ACM Comput. Surv.*, vol. 51, no. 1, p. 10, 2018.

[26] J. Wu, M. Dong, K. Ota, J. Li, and Z. Guan, "Big data analysis-based secure cluster management for optimized control plane in software-defined networks," *IEEE Trans. Netw. Service Manag.*, vol. 15, no. 1, pp. 27–38, Mar. 2018.

[27] K. Kenda, B. Kažič, E. Novak, and D. Mladenić, "Streaming data fusion for the Internet of Things," *Sensors*, vol. 19, no. 8, p. 1955, Apr. 2019.

[28] X. Lin, J. Li, J. Wu, H. Liang, and W. Yang, "Making knowledge tradable in edge-AI enabled IoT: A consortium blockchain-based efficient and incentive approach," *IEEE Trans. Ind. Informat.*, vol. 15, no. 12, pp. 6367–6378, Dec. 2019.

[29] U. A. Kashif, Z. A. Memon, S. Siddiqui, A. R. Balouch, and R. Batra, "Architectural design of trusted platform for IaaS cloud computing," *Int. J. Cloud Appl. Comput.*, vol. 8, no. 2, pp. 47–65, Apr. 2018.

[30] A. Fazli, A. Sayedi, and J. Shulman, "The effects of autoscaling in cloud computing," *Manage. Sci.*, vol. 64, no. 11, pp. 5149–5163, 2018.

[31] H. Liang, J. Wu, S. Mumtaz, J. Li, X. Lin, and M. Wen, "MBID: Micro-blockchain-based geographical dynamic intrusion detection for V2X," *IEEE Commun. Mag.*, vol. 57, no. 10, pp. 77–83, Oct. 2019.

[32] J. Wu, M. Dong, K. Ota, J. Li, and Z. Guan, "FCSS: Fog-computing-based content-aware filtering for security services in information-centric social networks," *IEEE Trans. Emerg. Topics Comput.*, vol. 7, no. 4, pp. 553–564, Oct. 2019.

[33] N. Wang, J. Li, D. Borisov, H. N. Gharti, Y. Shen, W. Zhang, and B. Savage, "Modeling three-dimensional wave propagation in anelastic models with surface topography by the optimal strong stability preserving Runge-Kutta method," *J. Geophys. Res. Solid Earth*, vol. 124, no. 1, pp. 890–907, 2019.

[34] S. Qiao, Q. Zhang, and Q. Zhang, "Mine fracturing monitoring analysis based on high-precision distributed wireless microseismic acquisition station," *IEEE Access*, vol. 7, pp. 147215–147223, 2019.

[35] J. Wu, M. Dong, K. Ota, J. Li, W. Yang, and M. Wang, "Fog-computing-enabled cognitive network function virtualization for an information-centric future Internet," *IEEE Commun. Mag.*, vol. 57, no. 7, pp. 48–54, Jul. 2019.

[36] J. Boakye, P. Gardoni, and C. Murphy, "Using opportunities in big data analytics to more accurately predict societal consequences of natural disasters," *Civil Eng. Environ. Syst.*, vol. 36, no. 1, pp. 100–114, Jan. 2019.

[37] S. C. Jaumé and L. R. Sykes, "Evolving towards a critical point: A review of accelerating seismic moment/energy release prior to large and great earthquakes," *Pure Appl. Geophys.*, vol. 155, nos. 2–4, pp. 279–305, 1999.

SHUAIQING QIAO was born in Shanxi, China, in 1993. He received the B.E. degree in measurement and control technology and instrumentation from the China University of Geosciences Beijing, in 2017, where he is currently pursuing the Ph.D. degree.

His main research interest includes the instrument science and technology.

QISHENG ZHANG was born in Anhui, China, in 1978. He received the M.S. and Ph.D. degrees from the Geosciences University of China, Beijing, China, in 2012.

He has been working with the School of Geo-Physics and Information Technology, China University of Geosciences, since 2005, where he is currently an Associate Professor. His research interests include system-on-a programmable-chip technology, measurement technology and instrument, high-precision data-converters, and geophysical instruments.

QIMAO ZHANG was born in Anhui, China, in 1987. He received the M.Sc. degree from the Geosciences University of China, Beijing, China, in 2012. He is currently a Research Assistant with the Institute of Electronics, Chinese Academy of Sciences (IECAS), Beijing.

FENG GUO was born in Taiyuan, Shanxi, China, in 1996. He received the B.E. degree in measurement and control technology and instrumentation from the China University of Geosciences, Beijing, in 2018, where he is currently pursuing the Ph.D. degree.

His main research interests are geodetection and information technology and instrumentation.

WENHAO LI was born in Zhumadian, Henan, China, in 1996. He received the B.E. degree in measurement and control technology and instrumentation from the China University of Geosciences, Beijing, in 2018, where he is currently pursuing the master's degree.

His main research interests are geophysical instruments and measurement technology and instrument.